

Mo+TiO₂(110) Mixed Oxide Layer: Structure and Reactivity

Osman Karshoğlu · Xin Song · Helmut Kuhlenbeck ·
Hans-Joachim Freund

© Springer Science+Business Media New York 2013

Abstract We present a STM/XPS/TPD/LEED study of the structural and electronic properties of Mo+Ti mixed oxide layers on TiO₂(110), and of their interaction with water, methanol and ethanol. Several different preparation procedures were tested and layers with different degrees of Mo/Ti mixing were prepared. Ordered mixed oxide surface phases with distinct LEED patterns could not be found; for all investigated Mo concentrations a TiO₂(110) like pattern was observed. Mo tends to agglomerate on the surface where it is found predominantly as Mo⁶⁺ at low coverages and as Mo⁴⁺ at high coverages. Mo⁴⁺ was also identified in the bulk of the mixed oxide layer. The Mo3d binding energies categorize the Mo⁴⁺ species as being dimeric. A third Mo3d doublet is attributed to a Mo species (Moⁿ⁺) with an oxidation state between those reported for Mo in MoO₂ and metallic Mo. Two types of Mo-induced features could be identified in the STM images for low Mo concentrations (in the range of 1 %). At higher Mo concentrations (~50 %) the surface is characterized by stripes with limited lengths in [001] direction. The concentration of bridging oxygen vacancies, which are common defects on TiO₂(110), is reduced significantly even at low Mo concentrations. Methanol and ethanol TPD spectra reflect this effect by a decrease of the intensity of the features related to these surface defects. At elevated MoO_x coverages, the yield of reaction products in methanol and ethanol TPD spectra are somewhat smaller than those found for clean TiO₂(110) and the reactions occur at lower temperature.

Keywords TiO₂(110) · Mo+Ti mixed oxide · Methanol adsorption · Ethanol adsorption

1 Introduction

Real catalysts are complex materials containing several components which renders the determination of their detailed structure challenging. The recipes of preparing industrial catalysts have historically been empirical rather than by design and understanding why a particular component results in a certain function of a catalyst is a difficult task. The difficulty stems simply from the vast number of possible interactions between the components, which scales factorially with the number of components. Even in the simple case of single oxides (M_xO_y), many types of surface defects such as vacancies, adatoms, line and plane defects, and reconstructions may create extreme complexity.

For mixed oxides (i.e. oxides containing more than one type of metal ion) it is well known since decades that cooperation of different components in catalytic processes may be essential [1, 2]. For example, the active site of a catalyst for the oxidation (ammoxidation) of propene to acrolein (acrylonitrile) contains neighboring bismuth and molybdenum sites, which each perform a specific function [3]. For some mixed oxide catalysts containing Mo, Bi, Sb, Sn, etc. it was reported that they operate with the so called “remote control” mechanism for selective oxidation reactions, in which one phase carries the active site and another phase regenerates the active site by adsorbing oxygen from the gas phase and transferring it to the active phase via spillover [1].

TiO₂ films prepared via sputtering techniques with a few per cent of molybdenum have proved to be more efficient for ethanol sensing than pure TiO₂ [4]. It was suggested

O. Karshoğlu · X. Song ·
H. Kuhlenbeck · Hans-Joachim Freund (✉)
Department of Chemical Physics, Fritz-Haber-Institut der
Max-Planck-Gesellschaft, Faradayweg 4-6,
14195 Berlin, Germany
e-mail: freund@fhi-berlin.mpg.de

that the main function of molybdenum is the inhibition of crystal coalescence. Also, recently theoretical studies of Mo-doped TiO₂ and Mo or MoO_x clusters supported on TiO₂ have appeared [5–9]. Kim et al. [5], using DFT calculations, have provided theoretical evidence that rutile doped with Mo (fivefold coordinated Ti surface atoms substituted by Mo and an extra O bound to it) has a lower energy for oxygen vacancy formation and a higher activity for CO oxidation via a Mars-van Krevelen mechanism than undoped TiO₂. Garcia-Mota et al. studied Mo doped TiO₂ with density functional techniques. Mo atoms were introduced at different substitutional sites and it was found that sixfold coordinated Mo is more stable than fivefold coordinated Mo at the surface. Mo substituted in the second layer under the bridging oxygen row was found to be the most stable configuration among the structures investigated, and this type of doped TiO₂ was proposed to result in the best performance for water splitting due to a lower overpotential. Kim et al. [7] investigated the dehydrogenation of methanol to formaldehyde on TiO₂ supported single MoO₃ clusters, again using DFT, and found that the activity of MoO₃ clusters is surpassed by that of VO₃.

In this paper we discuss strategies for the preparation of Mo+Ti mixed oxides and present results of structural and chemical surface characterizations. The mixed oxides were prepared in UHV as ultra-thin films with TiO₂ as the main component. Rutile-TiO₂ single crystals with (110) surface orientation were used as substrates, since in this case the overlayer-substrate lattice misfit is small which minimizes the interface strain. The films were characterized by scanning tunneling microscopy (STM), X-ray photoelectron spectroscopy (XPS), low-energy electron diffraction (LEED) and temperature programmed desorption (TPD).

2 Experimental

The experiments were performed in a commercial (Omicron) UHV system (base pressure $\sim 1 \times 10^{-10}$ mbar), which is equipped with room temperature STM, XPS, LEED, QMS, and a high pressure cell that is designed for the exposure of the sample to high pressures (up to 1 atm) in a temperature range from room temperature to ~ 900 K. Sample heating in the main chamber was performed by electron bombardment from a tungsten filament enclosed in a housing behind the sample. A tantalum plate was placed between the TiO₂(110) single crystal and the filament to avoid electron induced reduction of the oxide. O₂ was introduced to the chamber either by backfilling or via a gas doser (cylindrical tube with 10 mm inner diameter and a 20 μ m pinhole at some cm distance from the tube's end). The crystal was placed at ~ 1 –2 mm distance from the tube's end when dosing was performed. In this geometry

the effective O₂ pressure at the crystal surface is about two orders of magnitude higher than the O₂ pressure in the vacuum chamber. TiO₂(110) single crystals of $7 \times 8 \times 2$ mm³ size were purchased from Crystal GmbH, Germany. A K-type thermocouple was glued to the side of the crystal using Ultra-Temp 516 (Kager Industrieprodukte) ceramic glue (40 % Na₂SiO₃, 15 % ZrO₂, 45 % ZrSiO₄) for in situ temperature measurement. Commercial electron beam evaporators (Focus EFM3) were used for molybdenum and titanium evaporation. The deposition rates were calibrated using a quartz crystal microbalance. For most XPS measurements Al-K α (1486.6 eV) radiation and an Omicron EA125 electron energy analyzer were used. Additionally, some high-resolution spectra were obtained with synchrotron radiation from the UE52-PGM beamline of the BESSY II electron storage ring in Berlin using a Scienta SES 200 hemispherical electron energy analyzer. In the latter case the photon energies were chosen such that the kinetic energies of the photoelectrons from the studied core levels were ~ 100 eV in order to optimize the surface sensitivity. A part of the XPS spectra was recorded at grazing electron exit angles (70° or 80° with respect to the surface normal of the sample) in order to increase the surface sensitivity even further.

Molybdenum concentrations are given as cross-section weighted Mo3d XPS intensities divided by the sum of the cross-section weighted Mo3d and Ti2p XPS intensities in scans performed at an electron exit angle of 70° unless stated otherwise. A homogeneously mixed layer was assumed in the calculations of the concentrations, regardless of the actual structure. The transmission function of the analyzer was taken into account. STM images were taken using homemade W-tips prepared by alkali etching, in situ annealing and sputtering using a similar construction as the one described by Lyubinetsky et al. [10]. The images were processed with the WSxM software [11].

Temperature programmed desorption experiments were performed according to the following procedure: The sample was positioned in front of the gas doser after cooling it down to 110–120 K and ~ 10 L of the respective gas were dosed onto the surface. Hereafter the sample was heated up to 200 K in order to desorb the multilayer adsorbate followed by cooling down to ~ 130 K before positioning it in front of the QMS. TDS spectra were recorded for a temperature range of ~ 130 –800 K with a constant heating rate of 0.5 K/s. A smooth polynomial was subtracted from each spectrum as a baseline correction. Care was taken to avoid introduction of additional structures by this procedure.

The TiO₂ crystals were cleaned via repeated cycles of Ar sputtering (1,000 eV) at room temperature followed by a two-step annealing procedure. In the first step, the crystal was annealed at 970 K for 10–20 min in front of the gas

doser under a flow of oxygen gas in order to minimize crystal reduction. The oxygen pressure as measured with the ion gauge in the main chamber was 1×10^{-7} mbar which corresponds to a pressure in the 1×10^{-5} mbar range according to a simple estimate. This step results in the growth of large terraces [12]. The second step was annealing at 850 K in UHV for 10–15 min which removes the partially oxidized TiO_x clusters on the surface that form in the first step [13]. In all experiments reported here, the TiO_2 crystals had colors ranging from light blue to dark (but still transparent) blue, meaning that the majority of the bulk defects were point defects and not extended defects (like crystallographic shear planes) [14]. A (1×1) LEED pattern with a low background intensity was observed for surfaces prepared in this way.

3 Preparation of the Mixed Oxide Layers

TiO_2 (rutile, $P4_2/mnm$) and MoO_2 (monoclinic, $P2_1/c$, can be considered as “distorted” rutile) have similar structures and may be expected to mix to a certain extent. The mixed system has a miscibility gap below 1,400 K and Mo can be incorporated into the TiO_2 matrix only up to 5–6 % below 1,000 K [15]. Phase separation may be expected for higher Mo concentrations.

In our study four types of procedures were followed for the preparation of the “mixed” layers. These are illustrated schematically on a timeline in Fig. 1. In procedure 1 both metals were evaporated simultaneously in an atmosphere of 5×10^{-7} mbar of O_2 with the substrate being held at high temperature (≥ 800 K). In procedure 2, Mo was evaporated only in a small time window at about the middle of the Ti deposition period with the rest of the procedure being the same. This strategy was chosen in

order to “sandwich” the molybdenum between two layers of TiO_2 . The deposited layers were typically 10 monolayers (ML) thick for both procedures. The thickness of one monolayer is defined as the thickness of one layer of regular $\text{TiO}_2(110)$ [3.25 Å]. This definition is also applied to the mixed oxides, implicitly assuming that Mo atoms simply replace Ti atoms.

In the first step of procedure 3, Mo and Ti (in this order) are deposited onto TiO_2 at room temperature in UHV which prevents Mo oxidation (except for a slight oxidation due to TiO_2 reduction by Mo [16]) and traps the Mo atoms under a layer of Ti. This partially oxidized layer is then annealed in oxygen (15 min at 750 K in front of the gas doser with an effective pressure of $\sim 5 \times 10^{-7}$ mbar at the surface) to complete the oxidation process, and then in UHV (15 min at 800 K) to flatten the surface.

In procedure 4 a molybdenum oxide layer is prepared on $\text{TiO}_2(110)$. Mo is deposited onto TiO_2 in 5×10^{-7} mbar of O_2 at room temperature and then the sample is annealed to 800 K in UHV for 5 min.

4 Results and Discussion

MoO_x on $\text{TiO}_2(110)$ prepared according to procedure 4 is thermally stable up to at least 1,000 K. Fig. 2 shows a series of XPS spectra of a thin layer with 4.8 % Mo according to XPS. The sample was subjected to annealing in UHV for 15 min at 900, 950 and 1,000 K and XPS spectra were taken after each treatment. Neither changes the binding energy, nor the intensity of the Mo3d doublet.

Reported Mo3d binding energies of Mo in MoO_3 are in the $(235.8\text{--}235.6)/(232.7\text{--}232.5)$ eV range [17–20]. Slightly smaller binding energies of $(235.1/232.0)$ eV were obtained for a MoO_3 monolayer on Au(111) [20]. The

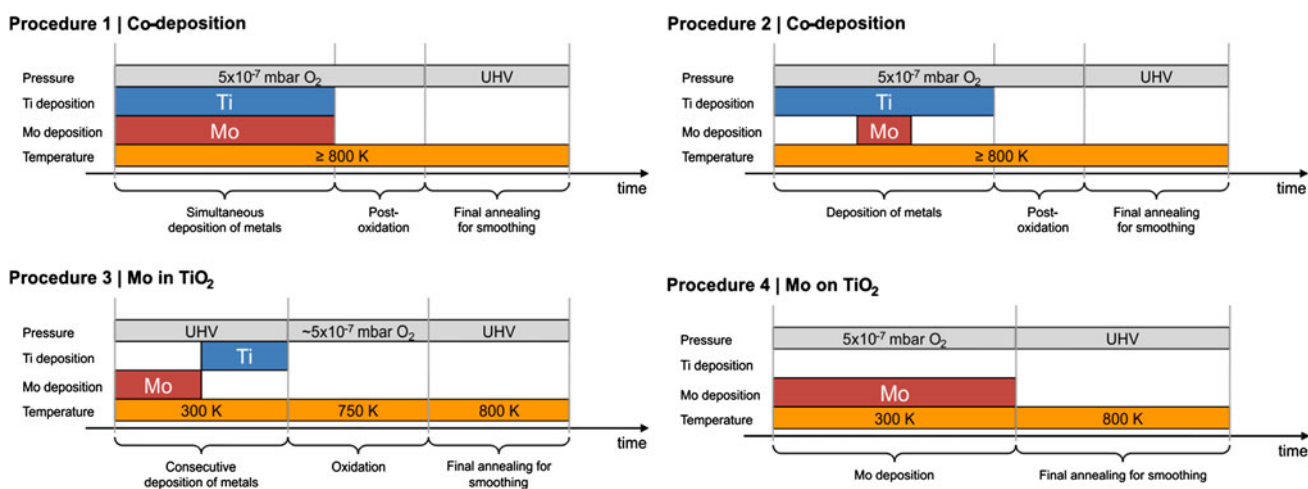


Fig. 1 Timeline representation of the four procedures which were used to prepare Mo–Ti mixed oxide layers

latter energies are identical to what is observed in Fig. 2, and therefore it appears reasonable to assign the Mo3d doublet in Fig. 2 to Mo^{6+} .

STM images of surfaces prepared according to procedure 4 with 1.3 % of Mo are presented in Fig. 3. These images show almost mono-disperse particles (X1) on the well-known $\text{TiO}_2(110)$ surface. In addition, “bright square” structures (X2) were identified. Figure 3c, d show these features on an enlarged scale. For X1, the minimum between the two lobes is situated above the 5cTi rows and between two 5cTi atoms while the center of the X2 features is above the titanium atoms under the row of bridging oxygen atoms. The structures of these two features are not yet understood. A system similar has been investigated by Chun et al. [22] with polarization-dependent total-reflection fluorescence X-ray absorption fine structure (PTRF-EXAFS). The authors deposited molybdenum onto $\text{TiO}_2(110)$ by impregnation of $(\text{NH}_4)_6\text{Mo}_7\text{O}_{24}$ and identified dimers of molybdenum oxide octahedra (edge-sharing) with the Mo–Mo axis being parallel to the $[1\bar{1}0]$ direction. The features denoted as X1 in our STM images may correspond to similar dimers. However, in our STM images the particles are centered at 5c Ti rows (bright rows in

STM) whereas the dimers proposed by Chun et al. are centered at bridging oxygen rows (dark rows in STM). Nevertheless, the size and the symmetry of the particles in Fig. 3 fit well with such a dimer model although the different positions indicate that there are issues with this interpretation. Calculations or further experiments may be required to shed light onto this problem.

Layers prepared according to procedures 1 and 2 with a low Mo concentration turned out to be very similar to layers that were prepared according to procedure 4: the Mo3d binding energies are identical in all cases and the relationships between the Mo concentrations calculated for 70° and 0° electron exit angles are very similar. Figure 4 shows the correlation between the Mo concentrations calculated from XPS data recorded at 70° and 0° electron exit angle for differently prepared layers. For Mo concentrations of up to $\sim 30\%$ the data for all three preparations follow the same functional dependence. In view of the limited diffusion speed of Mo in $\text{TiO}_2(110)$ one may safely assume that for the layer prepared according to procedure 4 all Mo is located at the surface. Since the concentrations determined for the layers prepared according to procedures 1 and 2 follow the same functional dependence we conclude that also in these cases the Mo is mainly located at the surface with a very limited bulk concentration. The result implies that Mo swims on the surface when the layers are prepared according to procedures 1 and 2 which both involve co-deposition of Mo and Ti in an oxygen ambient atmosphere. Procedure 2 even involves preparation of a titanium oxide layer on a Mo/Ti mixed oxide layer.

At x -axis values above 30 % in Fig. 4 the results for the different preparations start to differ, with significantly higher Mo concentrations observed at 0° electron exit angle for the layer prepared according to procedure 2, which may be an indication that for larger Mo concentrations some Mo can be stabilized in the bulk if the layer is prepared according to procedure 2. According to the phase diagram [15] at most 5–6 % of Mo can be solved in TiO_2 at 1,000 K under equilibrium conditions; under non-equilibrium conditions also higher concentrations are conceivable. We note that for high Mo surface coverages a non-linear functional dependence is expected and that the functional dependence will depend on the morphology of the MoO_x surface layer. Therefore another possible explanation for the differences in the results for the layers prepared according to procedures 1 and 2 may be that the morphologies of the Mo surface layers are different.

For layers prepared according to preparation procedures 1, 2 and 4 we always found that molybdenum seems to have a tendency to accumulate at the surface. We believe this has three main reasons: (i) deposition in O_2 oxidizes the Mo to Mo^{6+} and once formed, Mo^{6+} is trapped at the

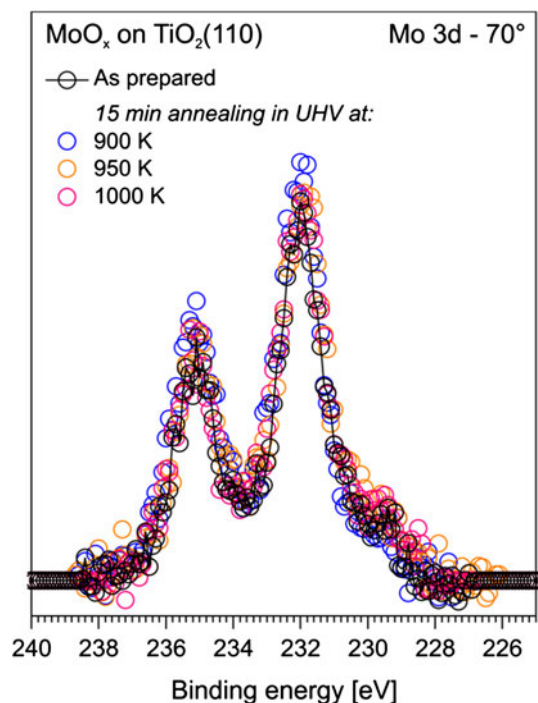


Fig. 2 Mo3d XPS (70° emission) spectra of a $\text{TiO}_2(110)$ surface with a thin MoO_x layer prepared according to procedure 4 with a Mo concentration of 4.8 %. The black line and the black circles represent the as-prepared surface. Colored circles represent the sample after annealing in vacuum as indicated in the figure. The intensities are not normalized. A Shirley-type background was subtracted from all spectra

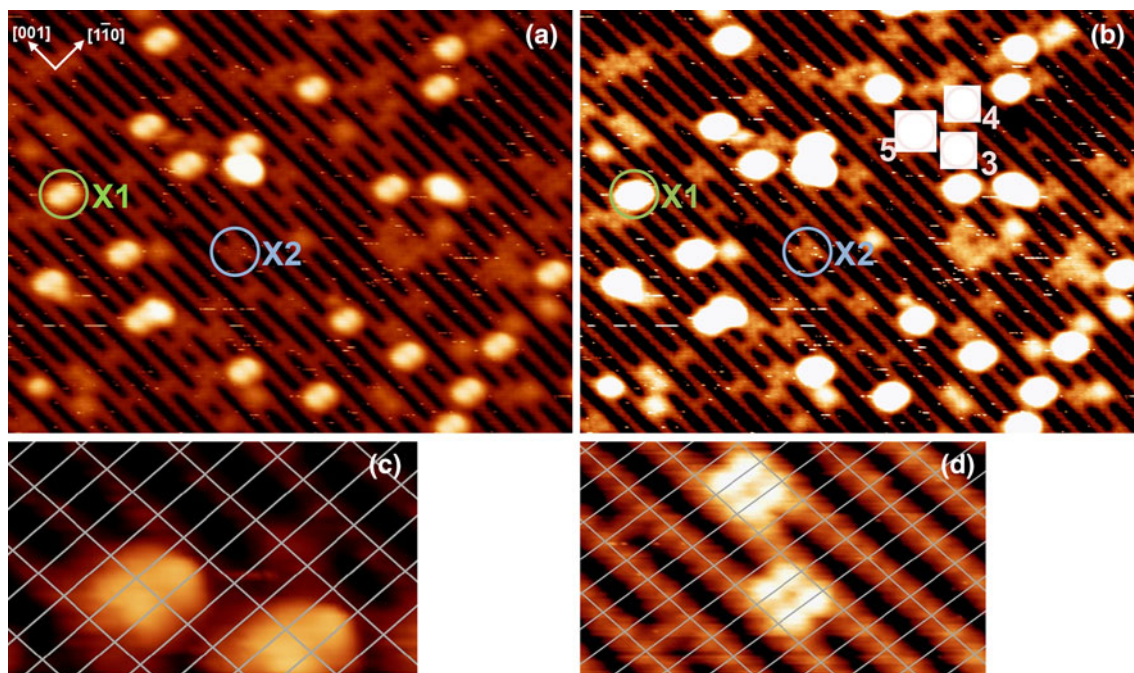


Fig. 3 STM images of a surface prepared according to procedure 4 with 1.3 % of Mo. Image (b) is identical to image (a) but with higher contrast, so that small protrusions are better visible. The two most common Mo-induced features are denoted by X1 and X2. Features 3, 4 and 5 are assigned to the well-known defects of $\text{TiO}_2(110)$ surfaces: bridging oxygen vacancies, hydroxyls and double hydroxyls respectively [21]. c, d Display X1 and X2 type structures on an *enlarged*

scale. The crossing points of the grid in c, d are positioned above the fivefold coordinated Ti atom sites. a Image size: $20 \times 15 \text{ nm}^2/\Delta U = +1.5 \text{ V}/I_t = 0.3 \text{ nA}$, full color scale 3.0 Å; b same as a but with full color scale of 1.0 Å, c $4.0 \times 2.3 \text{ nm}^2/\Delta U = +1.25 \text{ V}/I_t = 0.2 \text{ nA}$, full color scale 4.0 Å, d $4.6 \times 2.7 \text{ nm}^2/\Delta U = +1.25 \text{ V}/I_t = 0.2 \text{ nA}$, full color scale 1.0 Å

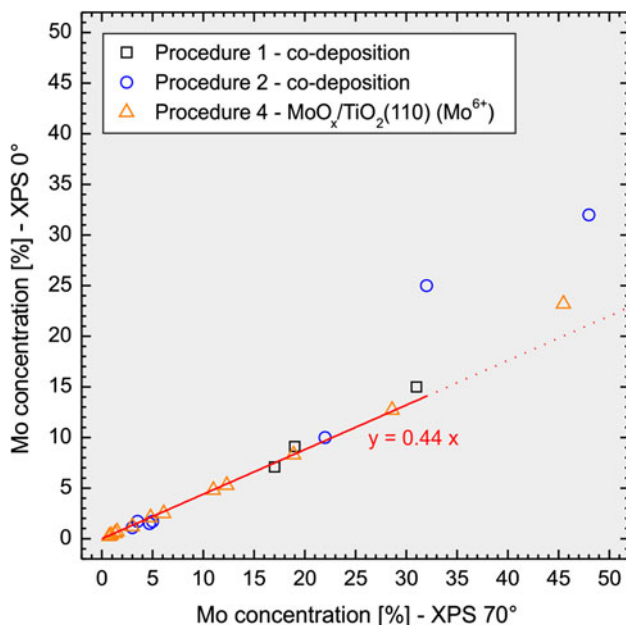


Fig. 4 Correlation of Mo concentrations as quantified by XPS spectra recorded at 70° (x-axis) and 0° (y-axis) electron exit angles for layers prepared according to procedures 1, 2, and 4

surface because it is probably more stable there than it is in the TiO_2 matrix where a 4+ oxidation state would likely be more appropriate; (ii) the larger ionic diameter of Mo as

compared to Ti ions [23] may make it energetically unfavorable to embed Mo ions into the TiO_2 lattice; (iii) deposition at high temperature may give enough surface mobility to the Mo ions so that they can avoid to be embedded into the layer when a film is grown by co-deposition (procedures 1 and 2). In order to overcome these issues, we prepared a mixed oxide layer according to procedure 3 where Mo deposition in vacuum is followed by Ti deposition in vacuum which is followed by oxidation via annealing in oxygen. The Mo layer plus the Ti layer of the prepared film contained material for 2 ML of oxide leading to $\sim 6.5 \text{ Å}$ thick oxide layer. For this layer the Mo3d binding energy is in the range reported for Mo^{4+} [17–19] which one may expect if Mo substitutes Ti in the rutile structure. The film was subjected to different annealing treatments in UHV and in an O_2 atmosphere. XPS spectra and STM images recorded after each step are shown in Fig. 5.

Figure 5 shows that annealing in UHV at 900 K does neither change the concentration nor the oxidation state of molybdenum while it flattens the surface and increases the size of terraces. The concentrations remain constant which implies that the diffusion of Mo in TiO_2 at 900 K is still fairly slow, at least at such low concentrations. Subsequent annealing in O_2 at 850 K leads to a Mo loss. Since the

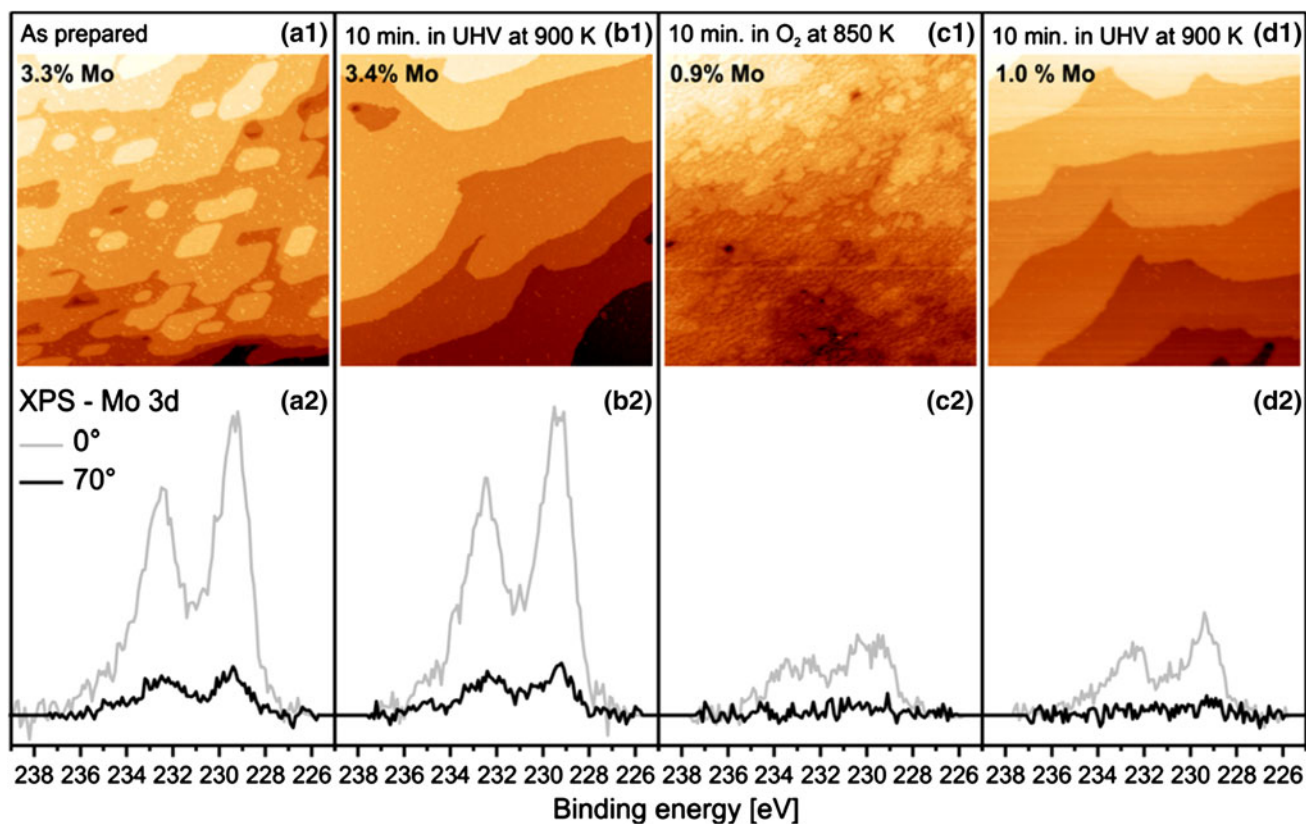


Fig. 5 STM images and corresponding Mo3d XPS spectra of two monolayers of Mo in TiO₂ prepared according to procedure 3. The Mo concentrations given in the STM images were determined from XPS spectra recorded for an electron exit angle of 0°. **a** After preparation of the layer, **b** after annealing in UHV at 900 K for 10 min, **c** after annealing at 850 K for 10 min in $\sim 5 \times 10^{-7}$ mbar

O₂ (effective pressure in front of the doser) followed by cooling down in O₂, **d** after annealing again in UHV at 900 K for 10 min. The preparation steps were performed consecutively from **a** to **d**. All STM images show an area of 200 × 200 nm² and were taken with $\Delta U = +1.25$ to 1.5 V and $I_t = 0.1$ –0.3 nA

diffusion of Mo into the TiO₂ bulk is slow we attribute this effect to the formation of new TiO₂ layers at the surface which are known to result from the oxidation of Ti interstitials which are the primary defects in reduced TiO₂ [24–26]. The STM images taken after oxidation (with cooling down in O₂) clearly show a corrugated morphology due to the new, partially formed layers. Annealing again in UHV at 900 K produces large flat terraces without changing the apparent concentration of Mo.

While the preparation procedures 1, 2, and 3 are attempts to prepare mixed oxide layers, procedure 4 is by design a method to grow Mo oxide layers on TiO₂(110). Figure 6a shows Mo3d XPS data of MoO_x layers with different thicknesses prepared according to procedure 4. Two doublets, which are assigned to Mo⁴⁺ and Mo⁶⁺ are identified in Fig. 6a. Peak fitting was applied to the spectra in order to quantify the relative amounts of the different oxidation states of Mo. The Mo3d peaks of Mo⁶⁺ were found to have symmetric shapes and therefore Voigt type symmetric functions were used for fitting while fitting the asymmetric Mo3d peaks of Mo⁴⁺ required the use of

asymmetric functions. We employed Gelius type functions as offered by the CasaXPS program [27]. The asymmetry parameters were determined by a fit of the data shown in Fig. 5a2 (Mo⁴⁺ in TiO₂). For both doublets a fixed spin-orbit splitting of 3.1 eV was assumed. Good quality fits with only two doublets (Mo⁶⁺ and Mo⁴⁺) could be obtained for Mo coverages of up to only 0.80 ML. The fits position the Mo3d levels of Mo⁶⁺ at (235.1/232.0 eV) with an uncertainty of 0.1 eV, and for Mo⁴⁺ the levels are found at (233.1/230.0 eV) for small coverages, shifting to (232.6/229.5 eV) for 1.55 ML. The areas of the fitted doublets are plotted as a function of MoO_x coverage in Fig. 6b. According to this plot, 6+ is the dominant Mo oxidation state at low coverage. Above 0.4 ML coverage, the amount of Mo⁶⁺ does not increase significantly, and Mo⁴⁺ becomes the dominant species (0.5 ML correspond to 1 Mo atom per TiO₂(110) unit cell). The findings can be explained by the following model: at low coverages Mo atoms are dispersed on the TiO₂ surface and have the highest possible number of oxygen coordination, and accordingly the highest oxidation state (Mo⁶⁺). As the

coverage increases, the extent of oxygen sharing among Mo atoms also increases and the film eventually converges to a MoO_2 -like structure, where the oxidation state of Mo is 4+. There is still some Mo^{6+} in the system which is located at the surface as shown in the following discussion.

The high-resolution Mo3d XPS spectra shown in Fig. 7 give a qualitative picture of the chemical composition, structure and thermal stability of a film grown according to procedure 1 where Mo and Ti are co-deposited in an ambient O_2 pressure at elevated temperature. Three distinct Mo3d doublets which are marked with colored lines can be identified in the spectra. The blue doublet is assigned to Mo^{6+} and the energy of the green doublet is in the energy range expected for Mo^{4+} . The red doublet is somewhere in between the binding energies for MoO_2 and Mo metal.

Quantitative analysis shows that the molybdenum concentration decreased from 48 to 14 % during annealing in oxygen which is largely attributed to sublimation of MoO_3 which is known to take place at 670 K for bulk-like MoO_3 layers on Au(111) [20]. Domenichini and co-workers also observed loss of molybdenum from Mo supported on $\text{TiO}_2(110)$, when the sample was heated to 800–1,000 K in

UHV [16]. It was shown that lattice oxygen of TiO_2 oxidized Mo to MoO_3 and this volatile oxide sublimated at high temperature [16]. This process was observed only for bulk stoichiometric, transparent yellow substrates, and not for bulk reduced, dark blue substrates.

From the dependence of the Mo3d intensities on the detection angle in Fig. 7, it is evident that the Mo^{6+} is located at the very surface and that the rest of the Mo species is concentrated below. Annealing the film in UHV at 800 K has barely any effect on the spectra. However, annealing in O_2 converts lower oxidation states to Mo^{6+} which is located at the surface as can be seen from a comparison of the highly surface-sensitive 80° spectrum with the less surface-sensitive 0° spectrum in Fig. 7c. Comparing the 0° spectra recorded before and after annealing in O_2 (Fig. 7a, c) additionally reveals a change in the relative intensities of the Mo species marked by green and red lines. The doublet marked by red lines becomes more dominant after oxidation which indicates that the species marked with the green lines is more prone to oxidation than the species marked with the red lines.

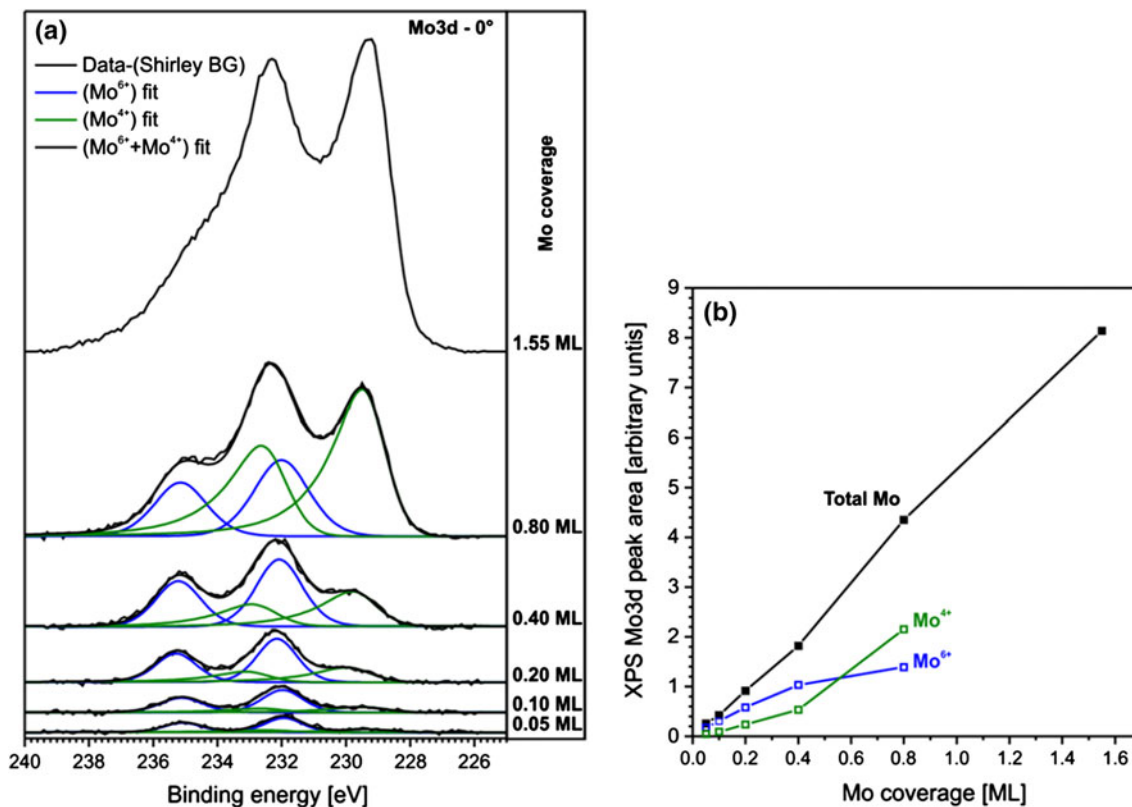


Fig. 6 **a** Mo3d XPS spectra (0° electron exit angle) as a function of Mo coverage from surfaces prepared according to procedure 4. Each surface was prepared by deposition of additional Mo onto the surface prepared in the previous step. The given coverages refer to the total amounts of Mo. Two doublets were fitted to the spectra representing Mo^{6+} and Mo^{4+} except for the highest coverage, where fitting with

only two doublets was found to be inappropriate. Details of the fitting procedure are given in the main text. **b** Intensities derived from the spectra are shown in **a** as a function of coverage. The *black line* is the integrated Mo3d signal after background subtraction. The intensity of the fitted Mo^{6+} doublet is the *blue line*, and the intensity of the fitted Mo^{4+} doublet is the *green line*

In order to assign the Mo^{4+} and Mo^{n+} peaks in Fig. 7, spectra of different preparations are compiled in Fig. 8 (see caption for explanations). The Mo3d binding energies for the two Mo^{4+} (green) containing samples (i.e. Mo in and on TiO_2) are in the range that is proposed for Mo-dimers [28, 29]. Dimer formation is not unlikely under our preparation conditions which involve heating to high temperatures. Dimer formation may also be the reason for the small diffusion speed of Mo in $\text{TiO}_2(110)$. Dimers of molybdenum are a common structural element in Mo complexes [30, 31] and they are also found in regular MoO_2 . Therefore their occurrence in the Ti+Mo mixed oxide system is not really surprising. The binding energies of the peaks marked with red lines are somewhere between those observed for MoO_2 and Mo metal. They are probably related to a compound which has stronger Mo–Mo bonds and an effective oxygen concentration smaller than that in MoO_2 . Domenichini et al. observed almost the same Mo3d binding energy when they deposited Mo on TiO_2 in UHV at submonolayer coverage. The red curve in Fig. 8 indicates that this species may also be formed at higher coverages.

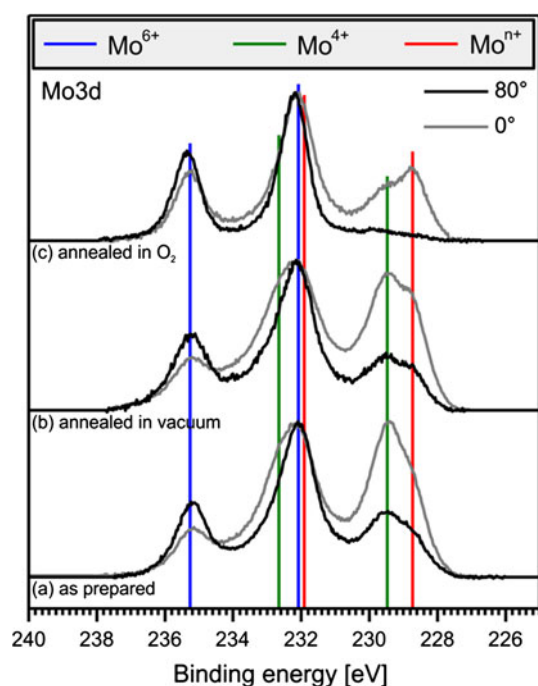


Fig. 7 High resolution XPS spectra of a Mo+Ti mixed oxide layer prepared according to procedure 1 at 800 K. The film thickness was about 50–60 Å and the Mo/Ti ratio was about 10 % as estimated from the calibration of metal deposition rates. XPS data taken at 0° electron exit angle yield a Mo content of 48 % for the as-prepared film. (a) As-prepared film, (b) after annealing in UHV at 800 K for 10 min, (c) after annealing in 1×10^{-6} mbar of O_2 for 20 min. The Mo concentration after the O_2 treatment decreased to 14 % as measured by XPS with 0° electron exit angle. All the curves were normalized to their maximum intensities after subtraction of a linear background

Mo dimers have also been proposed to exist in TiO_2 as “ Mo^{5+} dimers” [32]. We could not identify Mo^{5+} which is commonly reported in the electron paramagnetic resonance (EPR) literature for “Mo doped TiO_2 ” [32–35] which may be related to its low concentration which is well below the detection limit of XPS (<0.1 %) for Mo in the TiO_2 bulk [36]. There are reports of Mo^{5+} species on surfaces as well. These have been seen by XPS during reduction of supported (or unsupported) MoO_3 to MoO_2 but were never isolated as pure phases [37–39]. Deng et al. [40] identified Mo^{5+} at the shear planes of monolayer MoO_3 films grown on Au(111). We could not identify such a species, possibly because shear planes are not expected to form in noteworthy amounts under the chosen experimental conditions.

STM images of a different layer (but very similar to the layer whose Mo3d spectrum is shown in Fig. 7(b) in terms of concentration and chemical state of Mo) are presented in Fig. 9. Figure 9a, b provide complementary information regarding the structure of the surface. Figure 9b represents a large scale image ($500 \times 500 \text{ nm}^2$) which shows relatively wide terraces along with particles of 7–9 nm height and an irregular shape. The irregular shape of the particles is probably due to a convolution with the tip shape which

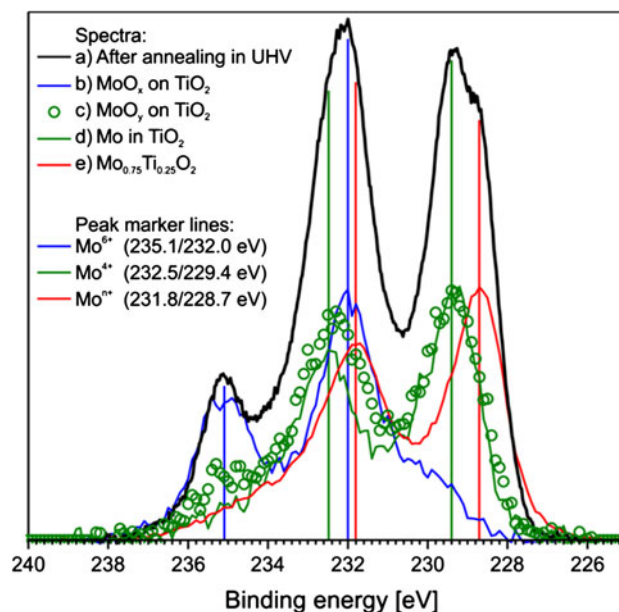


Fig. 8 Set of Mo3d XPS spectra recorded at 0° electron detection angle. (a) From Fig. 7: Mo+Ti mixed oxide layer prepared according to procedure 1 (Ti+Mo co-deposition in O_2) at 800 K (48 % Mo) and annealed for 10 min at 800 K in UHV; (b) Mo deposited onto TiO_2 in 5×10^{-7} mbar of O_2 at room temperature and post-annealed to 800 K in UHV for 5 min (11 % Mo, procedure 4); (c) Mo deposited onto TiO_2 in UHV at room temperature and post annealed to 670 K in UHV for 10 min (7.4 % Mo); (d) Mo embedded in TiO_2 (3.3 % Mo, procedure 3) from Fig. 5; (e) Mo-rich $\text{Mo}_{1-x}\text{Ti}_x\text{O}_2$ layer prepared according to procedure 1 at 800 K (75 % Mo)

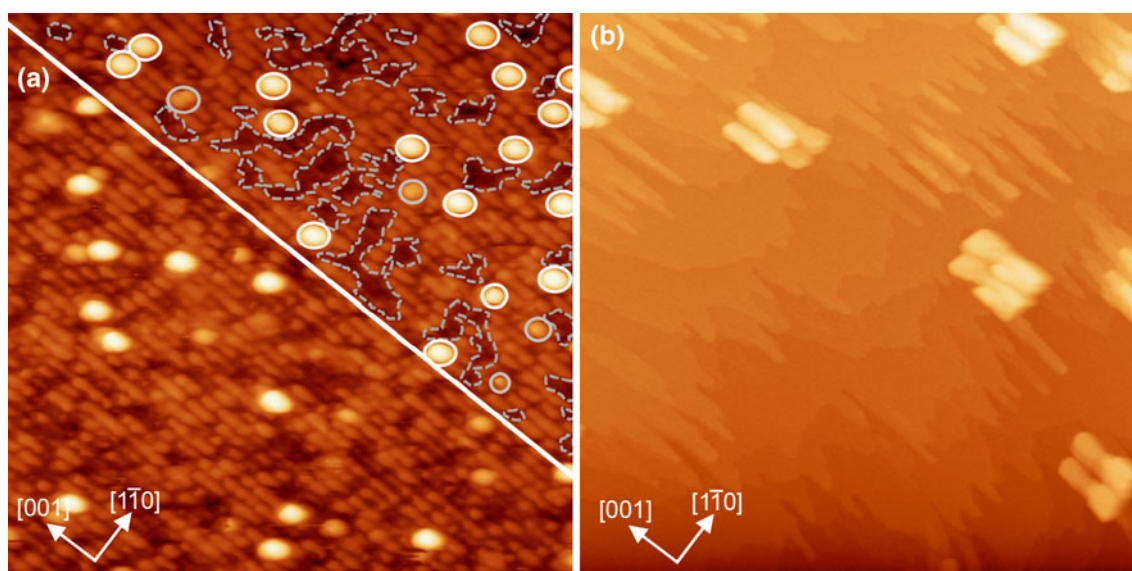


Fig. 9 STM images of a surface prepared according to procedure 1 at 870 K with a Mo concentration of 54 %. The film thickness is 33 Å (10 ML). **a** High resolution image from a terrace, $25 \times 25 \text{ nm}^2$, $\Delta U = +3.0 \text{ V}$, $I_t = 0.02 \text{ nA}$, full color range: 10 Å. In the upper right part of the image, regions of different heights have been marked. The regions enclosed by the *dashed grey lines* are the shallowest regions in the image and are taken as the base height for the

topography. The regions that are enclosed by *grey ellipses* are $\sim 5 \text{ Å}$ high and those by the *white ellipses* are $\sim 7.5 \text{ Å}$ high. The rest of the surface is $\sim 2.5 \text{ Å}$ high. **b** Large scale image revealing some large particles, $500 \times 500 \text{ nm}^2$, $\Delta U = +1.3 \text{ V}$, $I_t = 0.02 \text{ nA}$, full color range: 9 nm. The STM tip probably had a double apex giving rise to the appearance of duplicate structures

becomes especially relevant when the particle is smaller than the tip apex.

The STM image in Fig. 9a was taken on a terrace. There are features which are ~ 7.5 , ~ 5.0 and $\sim 2.5 \text{ Å}$ high relative to the regions of minimum height (these shallow parts of the surface are enclosed by dashed grey lines). 2.5 Å high regions cover a significant part of the image. 5.0 and 7.5 Å high features are isolated and marked with grey and white ellipses respectively. These features are partially the X1 type structures as marked in Fig. 3 but there some taller aggregates also.

The prepared layers all exhibit LEED patterns identical to that of $\text{TiO}_2(110)-(1 \times 1)$. IV LEED experiments were performed in order to check whether there is any indication of an ordered mixed oxide phase. Data are shown in Fig. 10 which compares IV curves of some diffraction spots of a mixed layer (16 % Mo, procedure 2) and clean $\text{TiO}_2(110)$. The IV curves are almost identical for the two different surfaces, which implies that there is no ordered Mo/Ti mixed oxide surface.

We could not identify any extended surface regions consisting of pure $\text{TiO}_2(110)$ and therefore we have to assume that the LEED spots stem from areas like the one shown in Fig. 9a. Part of the features seen in Fig. 9a may be due to structures also found on regular $\text{TiO}_2(110)$. In this sense the surface could be seen as heavily defected $\text{TiO}_2(110)$ and the LEED pattern would be that of $\text{TiO}_2(110)$, but with enhanced background intensity [41].

Figure 11 summarizes the structural aspects discussed up to here for layers prepared according to the procedures 1, 2 and 3. The components of the layers are: (i) surface MoO_x clusters, which contain Mo^{6+} or Mo^{4+} species depending on the size (small aggregates contain only Mo^{6+} while the Mo^{4+} concentration increases with increasing size), (ii) subsurface Mo, (iii) Mo^{4+} in TiO_2 in deeper layers. The large particles which are shown in Fig. 9b are not shown here since the material contained in them adds up to only a few per cent of a monolayer.

5 Interaction of $\text{MoO}_x/\text{TiO}_2(110)$ with Water and Alcohols

STM images and TPD spectra show that the coverage of bridging oxygen vacancies decreases when the MoO_x concentration increases. Figure 12 shows the coverages of three surface structures, namely bridging oxygen vacancies, X1 (particles) and X2 (bright square) as a function of the Mo concentration. For the determination of the oxygen vacancy concentration from STM images also hydroxyl groups were considered since they originate from the dissociation of water on oxygen vacancies.

Figure 12 quantitatively illustrates the steady decrease of the bridging oxygen vacancy concentration and the concomitant increase of the concentration of Mo induced features with increasing Mo concentration. The increase of

Fig. 10 Comparison of IV LEED curves of clean $\text{TiO}_2(110)$ and a mixed oxide layer with 16 % Mo prepared via Procedure 2. The LEED pattern was taken with 100 eV electrons from a clean TiO_2 surface

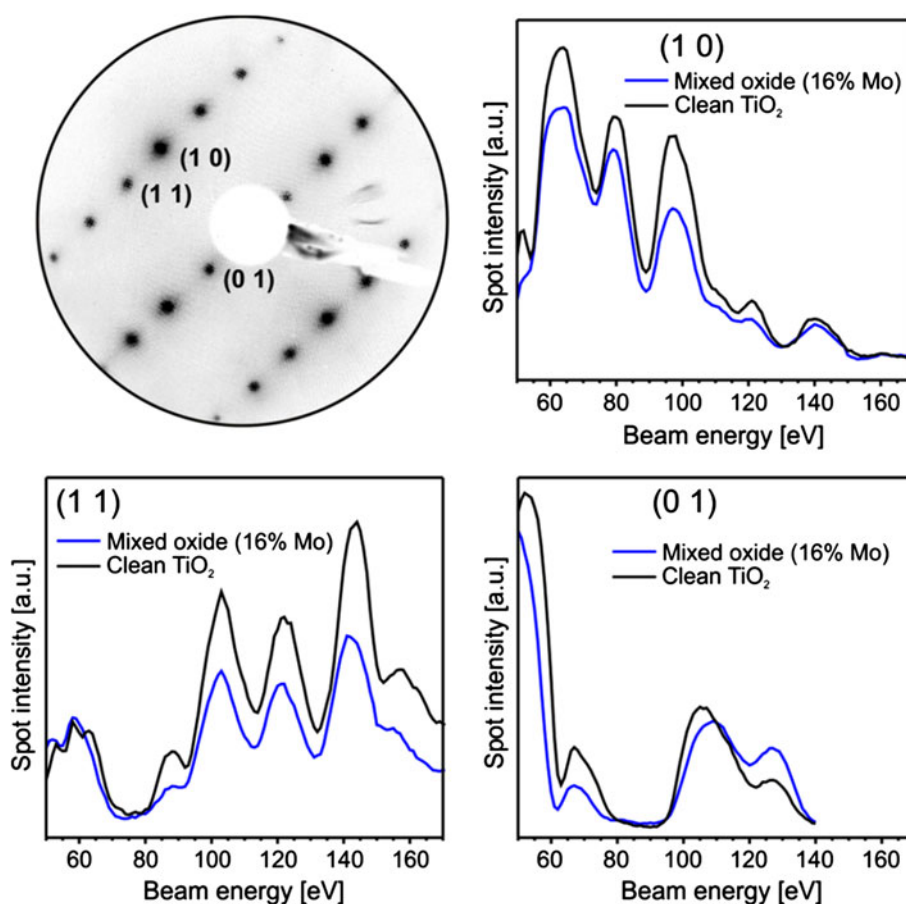
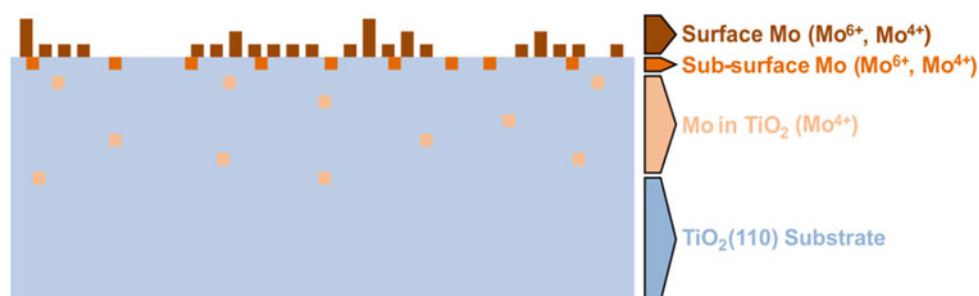


Fig. 11 Illustration of the structures that are proposed to form in/on a Mo+Ti mixed oxide layer. It is assumed that the layer is prepared according to procedure 1 or 2



the bright square concentration is faster in the beginning than the increase of the particle concentration but it slows down and at about 5 % Mo content, the concentrations of these two species become roughly the same. Small surface features like bridging oxygen vacancies, hydroxyl groups, and the Mo induced squares could not be reliably identified in STM images for Mo concentrations of more than $\sim 5\%$ and therefore corresponding values are missing in Fig. 12. A point to note is that the concentration of oxygen vacancies essentially reaches zero at Mo concentrations of more than 6 % which demonstrates that the Mo-induced features suppress oxygen vacancies.

Temperature programmed desorption spectra of water are shown in Fig. 13 for different Mo concentrations. The

high temperature desorption peak at about 500 K stems from the recombinative desorption of OH groups that form due to fission of water on the surface oxygen vacancy sites [43] while the peak at about 255 K is due to molecules desorbing from regular fivefold coordinated Ti sites [42–45]. The structure of the spectra changes with increasing Mo concentration. One aspect is that the intensity of the recombination peak at ~ 500 K decreases with increasing Mo concentration until it is essentially gone at a concentration of about 6 %, which is in good agreement with the vacancy concentration data shown in Fig. 12. Another aspect of the Mo induced changes is that the structures in the TPD spectra broaden when the Mo concentration rises. This is especially obvious in the top spectrum which is

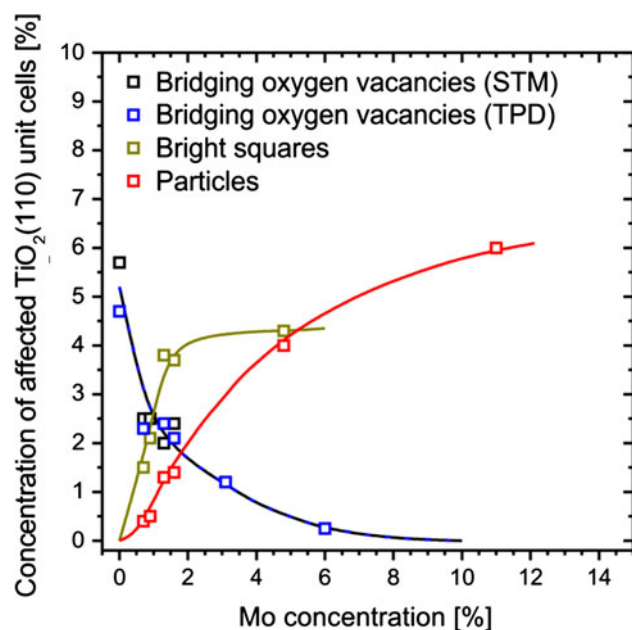


Fig. 12 Concentration of different surface features as a function of the molybdenum concentration. The concentrations were determined by counting the structures in the STM images and dividing this number by the total number of $\text{TiO}_2(110)-(1 \times 1)$ unit cells in the image. In the case of bridging oxygen vacancies, water TPD was additionally used for quantification. In this case the ratios of the intensities of the desorption peak at ~ 500 K (which is due to recombination of hydroxyl groups) and the H_2O monolayer desorption peak are plotted [42]. The molybdenum concentration was determined with XPS at 70° electron exit angle and is given relative to the concentration of metal ions in the sample, as described in the experimental part

from a surface with 44 % of Mo. We assign this effect to an increasing surface inhomogeneity. Figure 9a shows a STM image of a surface with a similar Mo concentration and it is clear that the morphology of this surface is more complex than that of regular $\text{TiO}_2(110)$. Part of the TPD structures at higher temperature is probably related to recombinative desorption of hydroxyl groups. Since the concentration of regular $\text{TiO}_2(110)$ surface vacancy sites is most likely significantly reduced at high Mo concentrations it follows that the surface likely exhibit sites involving Mo atoms which bind water and possibly also dissociate it.

TPD spectra of methanol for different Mo coverages are presented in Fig. 14. The desorption of methanol is accompanied by signals from smaller masses due to the cracking of methanol by the electron beam and surface reactions at the walls of the QMS and the QMS housing. These signals are especially prominent in the 200–400 K range where most of the methanol desorption takes place. While it is possible to account properly for the effect of cracking by the electron beam, this is not the case for the effect of the wall reactions. For this reason formaldehyde and methane signals are not shown for temperatures below 400 K. A significant part of the H_2O signal in this range is

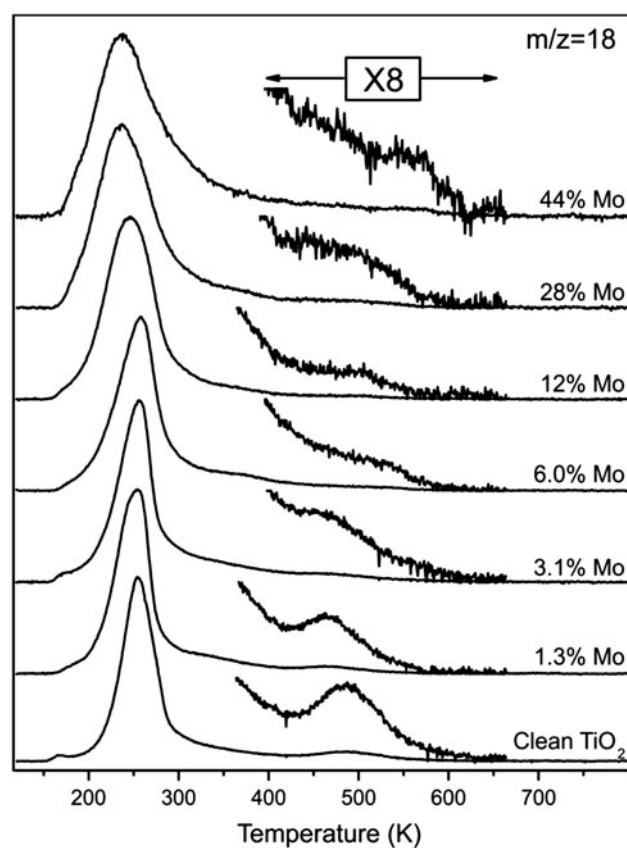


Fig. 13 Water TPD spectra for surfaces prepared according to procedure 4 with different molybdenum concentrations. Each mixed oxide surface was prepared by deposition of Mo onto the surface prepared in the previous step. The spectra are normalized to identical maximum intensities, since the QMS detection efficiency was found to vary somewhat between different measurements. A part of the spectra (around 500 K) was multiplied by a factor of 8 and is shown in addition

probably also related to wall reactions. As a rule of thumb we note that structures in the non-methanol spectra which are not found in the methanol spectra are most likely due to processes on the sample surface while this is not necessarily true for desorption maxima which are also found in the methanol spectra.

Prior studies identified three distinct methanol desorption features above 250 K for a clean $\text{TiO}_2(110)$ surface with bridging oxygen vacancies [46]. The peak at ~ 275 – 295 K and the shoulder at ~ 340 – 350 K were assigned to molecularly and dissociatively adsorbed methanol at $5c\text{Ti}$ sites, respectively, while the broad desorption feature at ~ 400 – 500 K was attributed to recombinative desorption of methanol dissociatively adsorbed at bridging oxygen vacancies [46].

At ~ 650 K parallel desorption of formaldehyde and methane takes place. This is different from previous studies which report formation of formaldehyde for oxygen treated $\text{TiO}_2(110)$ and methane desorption for electron bombarded,

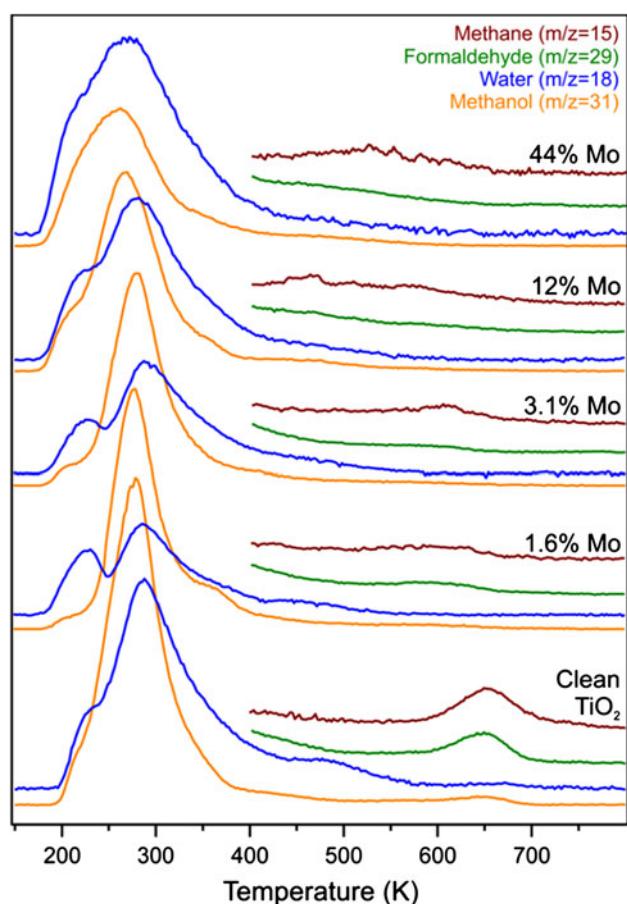


Fig. 14 TPD spectra of methanol-dosed surfaces prepared according to procedure 4 with different Mo concentrations. Each layer was prepared by depositing additional Mo onto the surface layer in the previous step. The spectra are normalized individually with the respective sensitivity factors. For water the intensity is scaled down by a factor of 0.35 in order to fit the spectra into the figure

highly oxygen deficient (i.e. reduced) $\text{TiO}_2(110)$ [46, 47]. We have TDS data from different samples which sometimes show co-desorption of formaldehyde and methane and sometimes neither of these is observed. This may be related to the history of the samples and/or the defect density. At present the existing data sets do not permit to discuss this issue in more detail.

Another interesting feature of our spectrum is the water desorption peak at ~ 490 K, which has not yet been reported for methanol on $\text{TiO}_2(110)$. Henderson reports that methanol TPD shows a “small amount of H_2O desorption” which was assigned to water adsorption from the residual gas atmosphere without stating the desorption temperature [46]. This explanation may also hold true for the data shown in Fig. 14 since the desorption temperature is identical to the temperature where recombinative water desorption occurs from a H_2O dosed surface as shown in Fig. 13. Another possible explanation would be that this desorption peak is due to the combination of hydroxyl

groups related to desorption of formaldehyde. The latter process involves the abstraction of two hydrogen atoms which in many cases desorb as water. The reason why, contrary to published results, methane and formaldehyde are produced in parallel is not clear. Methane production is not unexpected since the studied $\text{TiO}_2(110)$ surface surely contained vacancies. On the other hand, formaldehyde production is expected only for surfaces dosed with oxygen which was not the case for the studied surface. However, we note that Farfan-Arribas and Madix [47] did also observe formaldehyde production for a surface which they identified as “stoichiometric”. They assigned this to the use of oxygen in the course of the surface preparation.

Molybdenum heavily affects the high temperature desorption channels. Only 1.6 % of Mo induce a significant decrease of the intensities of the peaks at ~ 650 K. A general trend seems to be that the intensities are smeared out which is probably due to an inhomogeneous surface and that the reactions occur at lower temperature with a certain preference of methane formation at high Mo concentrations. If methane is produced then the oxygen atom of the methanol must remain on the surface (or is transferred to another reaction product which was not observed) which means that methane formation is accompanied by surface oxidation. We tentatively refer to Fig. 6b which shows that the concentration of Mo^{4+} increases with increasing Mo coverage. A possible explanation for the increasing amount of formed methane may be the oxidation of Mo^{4+} to a higher oxidation state. However, this speculation was not checked experimentally.

Kim et al. [7] investigated the dehydrogenation of methanol on monooxo MoO_3 clusters supported on $\text{TiO}_2(110)$ with DFT calculations and found a path towards formaldehyde with an activation energy of 1.40 eV. The rate determining step involves the breaking of a C–H bond, and the mechanism does not involve methoxy disproportionation. This activation energy inserted into the Arrhenius equation with a pre-exponential factor of 10^{12} s^{-1} yields a first order rate constant of 0.15 s^{-1} at 550 K. Redhead analysis [48] with an activation energy of 1.40 eV would correspond to a desorption peak temperature of about 520 K assuming the same pre-exponential factor. However, our TPD spectra show that only a small amount of formaldehyde produced in this temperature range which means that the process reported by Kim et al. [7] applies at most to a small part of the surface reactions.

Ethanol TPD spectra for the same substrates are presented in Fig. 15. The desorption products for ethanol on clean TiO_2 are similar to those published in the literature [49]. The features at ~ 295 and ~ 350 K are assigned to molecularly and dissociatively adsorbed ethanol at fivefold coordinated Ti sites, and the small feature at ~ 420 K is due to desorption of dissociatively adsorbed ethanol at

bridging oxygen vacancies. At ~ 600 K ethylene, acetaldehyde and water desorb together with additional ethanol.

Kim et al. [49] published TPD data of different alcohols (excluding methanol) on $\text{TiO}_2(110)$ which revealed that predominantly dehydration products (alkenes) are formed. Dehydrogenation products (aldehydes) are observed only for primary alcohols [49]. The most detailed mechanistic studies have been performed by Bondarchuk et al. [50] using 2-propanol, which revealed a previously unknown low-temperature dehydrogenation pathway. It was shown that the low-temperature mechanism does not require the presence of bridging oxygen vacancies whereas the high-temperature mechanism does [51].

A concentration of 1.6 % of Mo leads to a dramatic decrease of the amount of ethylene (as well as acetaldehyde, ethanol and water) at ~ 600 K, accompanied by a decrease in the peak temperature. The ethylene and formaldehyde yields decrease by ~ 50 % whereas the ethanol and water yield decreases by ~ 60 %. The numbers are in

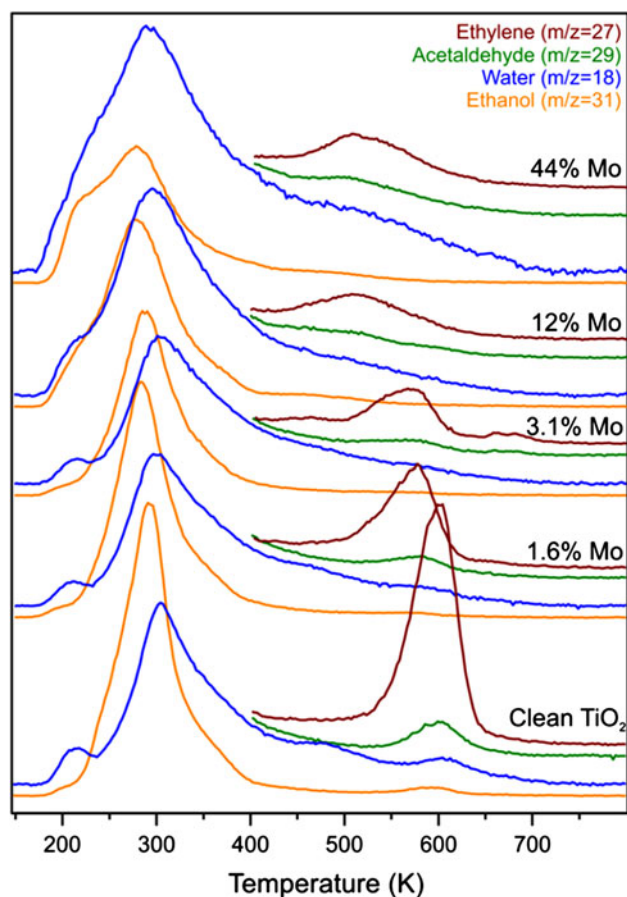


Fig. 15 TPD spectra of ethanol-dosed surfaces prepared according to procedure 4 with different Mo concentrations. Each surface was prepared by deposition of additional Mo onto the surface prepared in the previous step. The spectra are normalized individually with the respective sensitivity factors. For water the intensity is scaled down by a factor of 0.45 in order to fit the spectra into the figure

accordance with the decrease in the number of bridging oxygen vacancies (~ 50 %). With increasing Mo concentrations the structures become wider and shift to lower temperature with the ethylene desorption peak maximum finally reaching ~ 500 K.

The trend observed with increasing MoO_x coverage is the suppression of oxygen vacancy related chemistry of methanol and ethanol, which is in accordance with the independently determined decrease of the oxygen vacancy concentration (see Fig. 12). The shift of the high-temperature ethanol dehydrogenation product desorption peaks to lower temperature with increasing MoO_x coverage indicates the presence of new active sites. The number of these new active sites is likely smaller than the number of bridging oxygen vacancies on clean $\text{TiO}_2(110)$ as is evident from a simple comparison of the ethylene peak intensities.

6 Conclusions

$\text{Mo}+\text{Ti}$ mixed oxide layers and MoO_x layers were prepared on TiO_2 substrates using different procedures and characterized with XPS, STM and LEED. The LEED patterns of all preparations containing Mo were identical to the pattern of clean $\text{TiO}_2(110)$, except for variations of the background intensity. IV-LEED indicates that there are no ordered $\text{Mo}+\text{Ti}$ mixed oxide surface structures.

Based on detection-angle dependent XPS data it was found that molybdenum has the tendency to stay at the surface when Mo and Ti are co-deposited in an O_2 ambient (5×10^{-7} mbar) at high temperature (≥ 800 K) (procedure 1). This was the case even when additional Ti was deposited on top after Mo deposition (procedure 2), although some mixing of Mo into TiO_2 may be compatible with the data. Mixing of Mo into TiO_2 was achieved by consecutive deposition of Mo and Ti (in this order) in UHV at room temperature and subsequent oxidation at high temperature (procedure 3). Molybdenum mixed in $\text{TiO}_2(110)$ was found to have a oxidation state of 4+, consistent with a simple model where Mo substitutes Ti in the TiO_2 lattice. Mixed and non-mixed layers with low Mo concentrations were observed to be stable in UHV up to at least 900 and 1,000 K, respectively.

Mo^{6+} is the dominant oxidation state up to ~ 0.5 ML for layers prepared according to procedure 4. The amount of Mo^{6+} remained nearly constant for higher coverages while the amount of Mo^{4+} increases. Angle dependent XPS shows that Mo^{6+} is at the surface which favors a model where a MoO_2 -like structure terminated by Mo^{6+} species grows on TiO_2 .

In addition to Mo^{6+} and Mo^{4+} , also another Mo species (Mo^{n+}) was identified with XPS. The Mo3d doublet of the Mo^{4+} has binding energies typically associated with Mo

dimers in MoO₂, and therefore in the present case the doublet is also assigned to dimers. The Mo3d levels of the Moⁿ⁺ species are at binding energies between those found for MoO₂ and Mo metal. Its structure could not yet be characterized.

Annealing the films in O₂ at high temperature lead to two effects: (i) MoO_x species at the surface may be oxidized to MoO₃ which sublimates, (ii) new TiO₂ layers are formed via the oxidation of interstitial Ti atoms which are present in the bulk of TiO₂. The first effect removes Mo oxide that is on the surface and the second one damps the Mo3d intensity of Mo atoms already embedded in the TiO₂ lattice. Both effects result in a decrease of the apparent Mo concentration as determined from the Mo3d intensity.

Atomically resolved STM images of a layer with 1.3 % Mo were found to exhibit two Mo-induced features in addition to the features commonly observed for TiO₂(110). STM images of a layer with ~50 % Mo revealed a complex structure with irregularly shaped depressions (~2.5 Å deep) and small protrusions (~2.5 and ~5.0 Å high) with definite sizes. In addition, large particles with heights in the range of 7–9 nm were identified with a small concentration (~30 μm⁻²). A very simple structural model was proposed for co-deposited layers with a high Mo concentration.

Even small Mo concentrations result in a considerable decrease in the density of bridging oxygen vacancies which significantly affects surface reactions related to these defects since Mo inhibits the activity of TiO₂ even at low concentration. Mo+Ti related reactivity is characterized by lower reaction temperatures (as compared to pure TiO₂(110)) and wider and less structured TPD features which may be related to the increased surface inhomogeneity.

Acknowledgments We acknowledge support from the Deutsche Forschungsgemeinschaft (DFG) through SFB546 (Structure, Dynamics and Reactivity of Transition Metal Oxide Aggregates). Daniel Göbke, Mathias Naschitzki, and Elena Primorac are acknowledged for their support during a beamtime at the BESSY II electron storage ring.

References

- Pajonk GM (2000) Contribution of spillover effects to heterogeneous catalysis. *Appl Catal A* 202(2):157–169
- Weng LT, Delmon B (1992) Phase cooperation and remote-control effects in selective oxidation catalysts. *Appl Catal A* 81(2):141–213
- Grasselli RK, Burrington JD, Buttrey DJ, DeSanto P, Lugmair CG, Volpe AF, Weingand T (2003) Multifunctionality of active centers in (amm)oxidation catalysts: from Bi-Mo-O-x to Mo-V-Nb-(Te, Sb)-O-x. *Top Catal* 23(1–4):5–22
- Ferroni M, Guidi V, Martinelli G, Roncarati G, Comini E, Sberveglieri G, Vomiero A, Mea GD (2002) Coalescence inhibition in nanosized titania films and related effects on chemoresistive properties towards ethanol. *J Vac Sci Technol B* 20(2):523–530
- Kim HY, Lee HM, Pala RGS, Shapovalov V, Metiu H (2008) CO oxidation by rutile TiO₂(110) doped with V, W, Cr, Mo, and Mn. *J Phys Chem C* 112(32):12398–12408
- Garcia-Mota M, Vojvodic A, Metiu H, Man IC, Su HY, Rossmel J, Norskov JK (2011) Tailoring the activity for oxygen evolution electrocatalysis on rutile TiO₂(110) by transition-metal substitution. *ChemCatChem* 3(10):1607–1611
- Kim HY, Lee HM, Pala RGS, Metiu H (2009) Oxidative dehydrogenation of methanol to formaldehyde by isolated vanadium, molybdenum, and chromium oxide clusters supported on rutile TiO₂(110). *J Phys Chem C* 113(36):16083–16093
- Krüger P, Petukhov M, Domenichini B, Bourgeois S (2009) Molybdenum thin film growth on a TiO₂(110) substrate. *J Mol Struct Theochem* 903(1–3):67–72
- Asaduzzaman A, Krüger P (2007) Adsorption and diffusion of a molybdenum atom on the TiO₂(110) surface: a first-principles study. *Phys Rev B* 76(11):115412
- Lyubinetsky I, Yu ZQ, Wang CM, Du Y, Thevuthasan S (2008) Reproducible tip fabrication and cleaning for UHVSTM. *Ultramicroscopy* 108(9):873–877
- Horcas I, Fernandez R, Gomez-Rodriguez JM, Colchero J, Gomez-Herrero J, Baro AM (2007) WSXM: A software for scanning probe microscopy and a tool for nanotechnology. *Rev Sci Instrum* 78:013705
- McCarty KF (2003) Growth regimes of the oxygen-deficient TiO₂(110) surface exposed to oxygen. *Surf Sci* 543(1–3):185–206
- Li M, Hebenstreit W, Gross L, Diebold U, Henderson MA, Jennison DR, Schultz PA, Sears MP (1999) Oxygen-induced restructuring of the TiO₂(110) surface: a comprehensive study. *Surf Sci* 437(1–2):173–190
- Li M, Hebenstreit W, Diebold U, Tyryshkin AM, Bowman MK, Dunham GG, Henderson MA (2000) The influence of the bulk reduction state on the surface structure and morphology of rutile TiO₂(110) single crystals. *J Phys Chem B* 104(20):4944–4950
- Jacob KT, Shekhar C, Waseday Y (2008) Thermodynamic properties and phase diagram for the system MoO₂–TiO₂. *J Am Ceram Soc* 91(2):563–568
- Domenichini B, Flank AM, Lagarde P, Bourgeois S (2004) Interfacial reaction between deposited molybdenum and TiO₂(110) surface: role of the substrate bulk stoichiometry. *Surf Sci* 560(1–3):63–78
- Brox B, Olefjord I (1988) ESCA Studies of MoO₂ and MoO₃. *Surf Interface Anal* 13(1):3–6
- Werfel F, Minni E (1983) Photoemission-study of the electronic structure of Mo and Mo oxides. *J Phys C* 16(31):6091–6100
- Scanlon DO, Watson GW, Payne DJ, Atkinson GR, Egdell RG, Law DSL (2010) Theoretical and experimental study of the electronic structures of MoO₃ and MoO₂. *J Phys Chem C* 114(10):4636–4645
- Guimond S (2009) Vanadium and molybdenum oxide thin films on Au(111): growth and surface characterization. Humboldt Universität zu Berlin, Berlin
- Wendt S, Schaub R, Matthiesen J et al (2005) Oxygen vacancies on TiO₂(110) and their interaction with H₂O and O₂: a combined high-resolution STM and DFT study. *Surf Sci* 598(1–3):226–245
- Chun WJ, Asakura K, Iwasawa Y (1998) Polarization-dependent total-reflection fluorescence XAFS study of Mo oxides on a rutile TiO₂(110) single crystal surface. *J Phys Chem B* 102(45):9006–9014
- Shannon RD (1976) Revised effective ionic-radii and systematic studies of interatomic distances in halides and chalcogenides. *Acta Crystallogr A* 32:751–767

24. Henderson MA (1995) Mechanism for the bulk-assisted reoxidation of ion sputtered TiO₂ surfaces: diffusion of oxygen to the surface or titanium to the bulk? *Surf Sci* 343(1–2):L1156–L1160
25. Li M, Hebenstreit W, Diebold U (1998) Oxygen-induced restructuring of the rutile TiO₂(110)(1×1) surface. *Surf Sci* 414(1–2):L951–L956
26. Bowker M, Bennett R (2009) The role of Ti³⁺ interstitials in TiO₂(110) reduction and oxidation. *J Phys Condens Matter* 21(47):474224
27. CasaXPS (2006) Peak fitting in XPS. http://www.casaxps.com/help_manual/manual_updates/peak_fitting_in_xps.pdf
28. Grünert W, Stakheev AY, Morke W, Feldhaus R, Anders K, Shpiro ES, Minachev KM (1992) Reduction and metathesis activity of MoO₃/Al₂O₃ Catalysts. 1. An Xps investigation of MoO₃/Al₂O₃ catalysts. *J Catal* 135(1):269–286
29. Grünert W, Stakheev AY, Feldhaus R, Anders K, Shpiro ES, Minachev KM (1991) Analysis of Mo3d XPS spectra of supported Mo Catalysts: an alternative approach. *J Phys Chem* 95(3):1323–1328
30. Chae HK, Klemperer WG, Marquart TA (1993) High-nuclearity oxomolybdenum(V) complexes. *Coord Chem Rev* 128(1–2):209–224
31. Villata LS, Feliz MR, Capparelli AL (2000) Photochemical and catalytic properties of dimeric species of molybdenum(V). *Coord Chem Rev* 196:65–84
32. Meriaudeau P, Clerjaud B, Che M (1983) An electron-paramagnetic resonance study of Mo⁵⁺ pairs in polycrystalline TiO₂. *J Phys Chem* 87(20):3872–3876
33. Che M, Fichelle G, Meriaude P (1972) Paramagnetic absorption of pentavalent molybdenum in various symmetries of TiO₂. *Chem Phys Lett* 17(1):66–69
34. Kyi R (1962) Paramagnetic resonance of Mo⁵⁺ in TiO₂. *Phys Rev* 128(1):151–153
35. Meriaudeau P (1980) Paramagnetic-resonance of interstitial Mo⁵⁺ in a TiO₂ lattice. *Chem Phys Lett* 72(3):551–553
36. Valigi M, Gazzoli D, Jacono ML, Minelli G, Porta P (1982) A structural and magnetic study of the MoO_x-TiO₂ system. *Zeitschrift Fur Physikalische Chemie-Wiesbaden* 132(1):29–40
37. Quincy RB, Houalla M, Proctor A, Hercules DM (1990) Distribution of molybdenum oxidation-states in reduced Mo/TiO₂ catalysts: correlation with benzene hydrogenation activity. *J Phys Chem* 94(4):1520–1526
38. Yamada M, Yasumaru J, Houalla M, Hercules DM (1991) Distribution of molybdenum oxidation-states in reduced Mo/Al₂O₃ catalysts: correlation with benzene hydrogenation activity. *J Phys Chem* 95(18):7037–7042
39. Briand LE, Tkachenko OP, Guraya M, Wachs IE, Grünert W (2004) Methodical aspects in the surface analysis of supported molybdena catalysts. *Surf Interface Anal* 36(3):238–245
40. Deng X, Quek SY, Biener MM, Biener J, Kang DH, Schalek R, Kaxiras E, Friend CM (2008) Selective thermal reduction of single-layer MoO₃ nanostructures on Au(111). *Surf Sci* 602(6):1166–1174
41. Makinson JD, Lee JS, Magner SH, De Angelis RJ, Weins WN, Hieronymus AS (2000) X-ray diffraction signatures of defects in nanocrystalline materials. *Adv X-Ray Anal* 42(C):407–411
42. Li Z, Smith RS, Kay BD, Dohnálek Z (2011) Determination of absolute coverages for small aliphatic alcohols on TiO₂(110). *J Phys Chem C* 115(45):22534–22539
43. Henderson MA (1996) Structural sensitivity in the dissociation of water on TiO₂ single-crystal surfaces. *Langmuir* 12(21):5093–5098
44. Hugenschmidt MB, Gamble L, Campbell CT (1994) The interaction of H₂O with a TiO₂(110) surface. *Surf Sci* 302(3):329–340
45. Henderson MA (1996) An HREELS and TPD study of water on TiO₂(110): the extent of molecular versus dissociative adsorption. *Surf Sci* 355(1–3):151–166
46. Henderson M, Otero-Tapia S, Castro M (1999) The chemistry of methanol on the TiO₂ (110) surface: the influence of vacancies and coadsorbed species. *Faraday Discuss* 114:313–329
47. Farfan-Arribas E, Madix RJ (2003) Different binding sites for methanol dehydrogenation and deoxygenation on stoichiometric and defective TiO₂(110) surfaces. *Surf Sci* 544(2–3):241–260
48. Redhead P (1962) Thermal desorption of gases. *Vacuum* 12:203–211
49. Kim YK, Kay BD, White JM, Dohnálek Z (2007) Alcohol chemistry on rutile TiO₂(110): the influence of alkyl substituents on reactivity and selectivity. *J Phys Chem C* 111(49):18236–18242
50. Bondarchuk O, Kim YK, White JM, Kim J, Kay BD, Dohnálek Z (2007) Surface chemistry of 2-propanol on TiO₂(110): low- and high-temperature dehydration, isotope effects, and influence of local surface structure. *J Phys Chem C* 111(29):11059–11067
51. Kim YK, Kay BD, White JM, Dohnálek Z (2008) 2-Propanol dehydration on TiO₂(110): the effect of bridge-bonded oxygen vacancy blocking. *Surf Sci* 602(2):511–516